Stick-slip singularity of the Giesekus fluid

J.D. Evans*
Department of Mathematical Sciences, University of Bath,
Bath BA2 7AY, United Kingdom

July 20, 2014

Abstract

The local asymptotic behaviour at the stick-slip singularity is determined for the Giesekus fluid in the presence of a solvent viscosity. In planar steady flow, the method of matched asymptotic expansions is used to show that it comprises a three region structure. Specifically, an outer or core region that links boundary layers at the rigid stick and free slip surfaces. In the outer region, the velocity field is shown to be Newtonian at leading order, with solvent stresses dominating the polymer stresses. In terms of the radial distance r from the singularity at the join of the stick and slip surfaces, the velocity field vanishes as $O(r^{\frac{1}{2}})$. Consequently, the singular velocity gradients and solvent stresses are of $O(r^{-\frac{1}{2}})$ with the less singular polymer stresses being shown to be $O(r^{-\frac{5}{16}})$. The solvent and polymer stresses become comparable near the rigid stick and free slip surfaces, where boundary layers are required. These are of thickness $O(r^{\frac{5}{4}})$ at the rigid stick surface and thickness $O(r^{\frac{17}{14}})$ at the free slip surface. Solutions are constructed for both stick-slip and slip-stick flow regimes. These asymptotic results do not hold for the Oldroyd-B model nor for the case when the solvent viscosity is absent.

Keywords: Giesekus; solvent viscosity; stick-slip; boundary layers; stress singularity

* e-mail: masjde@maths.bath.ac.uk, Phone: +44 1225 386994, Fax: +44 1225 386492

1 Introduction

The extrusion of a viscoelastic jet from a die into an inviscid medium is an important situation occurring in polymer processing applications; see, for example, Tanner [33]. It is commonly referred to as the die-swell or extrudate-swell problem. The die may be a cylindrical pipe or a planar channel. Two characteristics of the die-swell problem are the expansion of the jet and the presence of a stress singularity at the exit of the die. The swelling of the extrudate for a viscoelastic fluid can be significantly more than that in the Newtonian case, see Tanner [32]. The presence of the stress singularity arises from the abrupt change in boundary conditions at the die exit. Its determination is crucial for understanding the extrudate-swell phenomenon as discussed by, for example, Andre and Clermont [1] and Tanner [32, 34].

A simplified version of the die-swell problem is the the so called stick-slip problem. Here the free surface is now fixed as a smooth continuation of the die wall with the swelling effect suppressed. Tanner and Huang [35] describe its possible setup through consideration of a repeating pattern of equally spaced channel walls. It is a situation in which the stress singularity at the die lip can be investigated and may be regarded as a first step toward understanding the more involved die-swell problem. It is emphasised that the term stick-slip is used here in regard to the change in the boundary conditions as the fluid leaves the pipe/channel and not to experimentally observed spurt flow with the extrudate exhibiting alternate smooth and sharskin regions, see, for example Denn [5].

In the Newtonian case, the stick-slip problem for Stokes flow (absence of inertia) was completely solved by Richardson [27] in the planar case and Trogdon and Joseph [36] in the 3-d axisymmetric case. For Newtonian fluids it may be considered to arise in the limit of large surface tension. Both sets of authors exploited the problem linearity and strip geometry by using the Weiner-Hopf technique, with in addition Trogdon and Joseph showing consistency with a matched eigenfunction expansion approach. The more general die-swell problem for a Newtonian fluid, has been considered analytically by Solonnikov [31].

For viscoelastic fluids, there is a paucity of analytical results and the question of well-posedness for these problems is an open issue. Further, numerical simulation tends to be problematic, see for example Lipscombe et al. [20] and Fortin et al. [10] for difficulties encountered in earlier numerical work. This has been attributed to the highly singular stresses encountered. Consequently both numerical and analytical work near the singularity has seen either the modification of the viscoelastic constitutive equations or the introduction of slip on the die walls. For example, Apelian et al. [2] and King et al. [18] use the Modified UCM model in place of UCM or Oldroyd-B models, whilst slip on the die walls has been used by Salamon et al. [28] for the Oldroyd-B model (and Silliman and Scriven [30] for a Newtonian fluid). A comprehensive summary of the schemes and viscoelastic models simulated for stick-slip and die-swell can be found in Ngamaramvaranggul and Webster [24] and more recently in Karapetsas and Tsamopoulos [16, 17]. Analytically, Tanner and Huang [35] used an adaption of the J-integral approach from fracture mechanics to deduce that the singularity behaviour for Phan-Thien–Tanner (PTT), Modified Upper Convected Maxwell Model (MUCM) and general network models were of Newtonian form. Nothing definitive could be said for UCM and Oldroyd-B flows. (The approach usefully allowed the singularity intensity factors to be deduced for Newtonian and generalised Newtonian (particularly power law) fluids). Fontelos and Friedman [9] obtained existence and uniqueness results for a class of Oldroyd models (that don't include the B and A variants) in stick-slip.

Our focus here will be determining the stress singularity at the die exit for stick-slip flow and the Giesekus viscoelastic model. The Giesekus model [12, 13], is a class of constitutive equations based on anisotropic drag and the concept of a deformation dependent tensorial mobility of dissolved molecules. It describes how the relaxation time of a molecule (elastic dumbbell) is altered when the surrounding molecules (elastic dumbbells) are oriented. The relaxation behavior becomes anisotropic and results in an additional quadratic term of the stress tensor compared to the Maxwell model. A better description of polymeric solutions and melts is obtained, than for some other rheological models such as the Oldroyd-B model or corotational model. It enables a qualitative description of a number of well-known properties of viscoelastic fluids, namely shear thinning, non-zero second normal stress coefficient and stress overshoot in transient shear flows; see Giesekus [14], Larson [19] and Bris et al. [4].

Currently, the Giesekus model has not received attention within such an analytical study. The approach

will use the method of matched asymptotic expansions that was successfully use by Evans [8] for the affine PTT model. It may be anticipated that its behaviour should be similar to the PTT model, since both involve quadratic stress terms. The main results of the paper will show that on small radial distances r near to the singularity:

1. The stress field is Newtonian dominated. Away from the stick and slip surfaces, the solvent stresses thus dominate and are $O(r^{-\frac{1}{2}})$ whilst the polymer stresses are $O(r^{-\frac{5}{16}})$ (which compare to $O(r^{-\frac{4}{11}})$ for PTT).

2. A boundary layer of thickness $O(r^{\frac{5}{4}})$ is required at the stick surface to accommodate viscometric flow. This thickness should be compared with $O(r^{\frac{7}{6}})$ for PTT.

3. A boundary layer of thickness $O(r^{\frac{17}{14}})$ is required at the slip surface to arrest elongational growth of the stresses. This thickness compares with $O(r^{\frac{23}{20}})$ for PTT.

Thus the polymer stress is less singular than that obtained for PTT, but the boundary layers are correspondingly narrower than their PTT counterparts. This is a trend that was identified for the high Weissenberg number boundary layers of Hagen and Renardy [15] and re-entrant corner behaviour discussed in Evans [6, 7]. Crucial to these results is the presence of a solvent viscosity and the quadratic stress terms. The solvent viscosity has a regularizing effect on the model behaviour, with the polymer stresses less singular than the solvent stresses. The presence of the quadratic stress terms arrest the strong stress growth that occurs in elongational flow after the die exit. The loss of either of these effects from the model is sufficient to significantly change the asymptotic behaviour at the singularity, which currently remains unknown.

The advantages of determining the stress singularity are several. First it is a test of the rheology, to see how the constitutive equations behave under large stresses. Second, the form of the singularity is of use to numerical schemes, where it's behaviour can be incorporated to improve accuracy. This is particularly important for viscoelastic models which have strong hyperbolic properties that tend to propagate inaccuracies along streamlines. This has successfully been done for Newtonian fluids, where Georgiou et al. [11] introduced singular finite elements in the vicinity of the singularity to improve the solution accuracy and speed up the rate of convergence. However, this approach relies upon knowing the analytical form of the singularity. Thirdly, it adds to a catalogue of reference behaviours.

The problem formulation is introduced in section 2, where the governing equations, boundary conditions and their non-dimensionalisation is detailed. The details of the asymptotic analysis are then given in section 3. The analysis is performed in both the Cartesian and natural stress formulations of the constitutive equations. The most efficient approach for the analysis is using natural stress variables, where the link between solutions in the asymptotic regions occurs at leading order. However, performing the analysis in Cartesian variables is useful as it provides a consistency check on the natural stress results and is arguably easier to interpret physically particularly near the boundaries. However, it does suffer from requiring higher order terms in the outer expansions to communicate the correct stress information between the stick and slip surfaces. It is thus advantageous to record the details for both formulations. Finally in section 4 a summary of the results in dimensional form is given.

2 Problem formulation

The geometry for classical stick-slip flow is depicted in Figure 1 for the planar channel case. The channel width is taken as $2H$, with an assumed incoming plane Poiseuille flow far upstream with mean speed V. The fluid exits the channel at $x = 0$, far downstream of which it has a fully developed (shear-free) plug flow. If we take the speed of the plug flow as V, then the Poiseuille flow takes the form

$$\mathbf{v} = \left(3V\frac{y}{H}\left(1-\frac{y}{2H}\right), 0\right) \tag{2.1}$$

which follows from mass conservation through a flux balance for the two flows. The reverse flow set-up of slip-stick will also be considered. This being more for mathematical interest rather than practical.

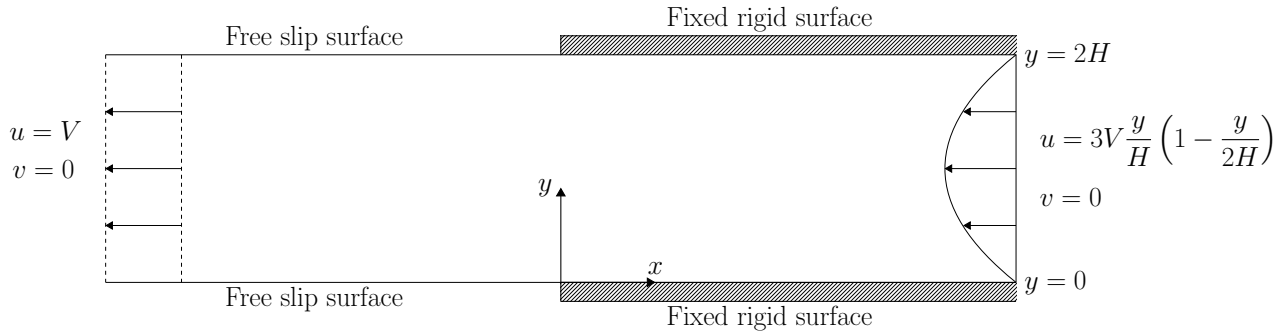

Figure 1: Stick-slip problem for a planar channel of width $2H$. Incoming Poiseuille flow upstream and shear-free plug flow downstream.

The governing equations for steady incompressible planar flow of the Giesekus fluid are written in dimensional slow flow form

$$\nabla \cdot \mathbf{v} = 0, \qquad 0 = -\nabla p + \nabla \cdot \boldsymbol{\tau}, \tag{2.2}$$

where $\mathbf{v} = (u, v)^T$ is the velocity field (represented by the usual 2-D stream function ψ) and p the pressure. The extra stress tensor $\boldsymbol{\tau} = \boldsymbol{\tau}^s + \boldsymbol{\tau}^p$ consists of a Newtonian solvent contribution $\boldsymbol{\tau}^s$ and an elastic polymeric contribution $\boldsymbol{\tau}^p$. The solvent stress is given by

$$\boldsymbol{\tau}^s = 2\eta_s \boldsymbol{D}, \tag{2.3}$$

where η_s is the solvent viscosity and $\mathbf{D}$ is the rate of strain (or deformation rate) tensor given by

$$\mathbf{D} = \frac{1}{2}(\nabla \mathbf{v} + (\nabla \mathbf{v})^T). \tag{2.4}$$

The extra elastic stress tensor $\boldsymbol{\tau}^p$ is taken to satisfy the Giesekus constitutive equation

$$\boldsymbol{\tau}^p + \lambda \left(\overset{\triangledown}{\boldsymbol{\tau}}^p + \frac{\alpha_{\text{mob}}}{\eta_p} (\boldsymbol{\tau}^p)^2 \right) = 2\eta_p \mathbf{D}, \tag{2.5}$$

where λ is the stress relaxation time, α_{mob} is the mobility parameter of the model, η_p the polymer viscosity and the upper convected derivative of the elastic stress being

$$\overset{\triangledown}{\boldsymbol{\tau}}^p = (\mathbf{v} \cdot \nabla)\, \boldsymbol{\tau}^p - (\nabla \mathbf{v})\, \boldsymbol{\tau}^p - \boldsymbol{\tau}^p\, (\nabla \mathbf{v})^T .$$

The mobility parameter takes values in the range $0 \leq \alpha_{mob} \leq 1$ and determines the magnitude of the anisotropic drag modelled by the presence of the quadratic stress term. Bird et al. [3] and Schleiniger and Weinacht [29] noted that realistic behaviour is usually observed for $0 < \alpha_{\text{mob}} < 0.5$. Boundary conditions are taken of no-slip and solid boundary on the channel walls

$$\text{at } y = 0, 2H \text{ for } x > 0, \qquad u = v = 0, \tag{2.6}$$

with no shear stress and no normal component of velocity on the free surface

$$\text{at } y = 0, 2H \text{ for } x < 0, \qquad \tau_{12} = 0, \quad v = 0. \tag{2.7}$$

The subscripts of the Cartesian stress components having their usual meaning of 1 for the x direction and 2 for the y direction. The problem statement is completed with suitable consistent stress conditions specified for the incoming Poiseuille flow far upstream and the fully developed plug flow far downstream.

This system of equations is nondimensionalised as follows

$$\mathbf{x} = H\bar{\mathbf{x}}, \qquad \mathbf{v} = V\bar{\mathbf{v}}, \qquad p = (\eta_s + \eta_p)\frac{V}{H}\bar{p}, \qquad \boldsymbol{\tau} = (\eta_s + \eta_p)\frac{V}{H}\bar{\mathbf{T}}, \qquad \boldsymbol{\tau}^s = \frac{\eta_s V}{H}\bar{\mathbf{T}}^s, \qquad \boldsymbol{\tau}^p = \frac{\eta_p V}{H}\bar{\mathbf{T}}^p,$$

using the channel half-width H and mean speed V as characteristic length and flow speeds respectively. Dropping bars, we thus obtain the dimensionless governing equations as

$$\nabla \cdot \mathbf{v} = 0, \qquad 0 = -\nabla p + \beta \nabla \cdot \mathbf{T}^s + (1-\beta)\nabla \cdot \mathbf{T}^p, \tag{2.8}$$

$$\mathbf{T}^s = 2\mathbf{D}, \qquad \mathbf{T}^p + \mathrm{Wi}\left(\overset{\triangledown}{\mathbf{T}}^p + \kappa(\mathbf{T}^p)^2\right) = 2\mathbf{D}, \tag{2.9}$$

with total extra stress $\mathbf{T} = \beta\mathbf{T}^s + (1-\beta)\mathbf{T}^p$. The dimensionless parameters are the Weissenberg number Wi, Newtonian solvent viscosity β and model parameter κ defined as

$$\mathrm{Wi} = \frac{\lambda V}{H}, \qquad \beta = \frac{\eta_s}{\eta_s + \eta_p}, \qquad \kappa = \alpha_{\mathrm{mob}}.$$

The introduction of κ is purely for convenience and notational consistency with the high Weissenberg boundary layer equations of Hagen and Renardy [15], which will be seen to play a key role. It is convenient to scale the solvent and polymer extra stresses with their respective viscosities, rather than the total viscosity $\eta_s + \eta_p$. This has the effect of removing the dimensionless solvent viscosity parameter β from both dimensionless constitutive equations as stated in (2.9). The boundary conditions (2.6)–(2.7) become, non-dimensionally,

$$\text{at } y = 0 \qquad \begin{cases} u = v = 0, & \text{for } x > 0, \\ T_{12} = v = 0, & \text{for } x < 0, \end{cases} \tag{2.10}$$

with a similar statement at $y = 2$. Our goal is to determine the behaviour of the equations (2.8)–(2.9) near to the join of the stick and slip surfaces where a change in the boundary conditions occurs as given by (2.10). This change in the boundary condition gives rise to singularities in the velocity gradients and stresses, the form of which we seek to elucidate. We focus on the behaviour near the stated origin, with similar singular behaviour occuring at the point $(0, 2)$. When necessary we use polar coordinates (r, θ) centered at the origin, with the solid stick surface being $\theta = 0$ and the free slip surface $\theta = \pi$. The asymptotic analysis presented holds for the parameter ranges

$$\mathrm{Wi} = O(1), \qquad 0 < \beta \leq 1, \qquad 0 < \kappa < 1.$$

It excludes the no solvent viscosity case $\beta = 0$ and the Oldroyd-B model $\kappa = 0$, both of these limits being singular for the solution constructed here.

For later reference, we state the polymer stress constitutive equation in (2.9) in both Cartesian and natural stress forms. Both formulations will be useful in the analysis. In Cartesian form the constitutive equations are

$$T^p_{11} + \mathrm{Wi}\left(\frac{\partial\psi}{\partial y}\frac{\partial T^p_{11}}{\partial x} - \frac{\partial\psi}{\partial x}\frac{\partial T^p_{11}}{\partial y} - 2\frac{\partial^2\psi}{\partial x\partial y}T^p_{11} - 2\frac{\partial^2\psi}{\partial y^2}T^p_{12} + \kappa\left((T^p_{11})^2 + (T^p_{12})^2\right)\right) = 2\frac{\partial^2\psi}{\partial x\partial y}, \tag{2.11}$$

$$T^p_{22} + \mathrm{Wi}\left(\frac{\partial\psi}{\partial y}\frac{\partial T^p_{22}}{\partial x} - \frac{\partial\psi}{\partial x}\frac{\partial T^p_{22}}{\partial y} + 2\frac{\partial^2\psi}{\partial x\partial y}T^p_{22} + 2\frac{\partial^2\psi}{\partial x^2}T^p_{12} + \kappa\left((T^p_{12})^2 + (T^p_{22})^2\right)\right) = -2\frac{\partial^2\psi}{\partial x\partial y}, \tag{2.12}$$

$$T^p_{12} + \mathrm{Wi}\left(\frac{\partial\psi}{\partial y}\frac{\partial T^p_{12}}{\partial x} - \frac{\partial\psi}{\partial x}\frac{\partial T^p_{12}}{\partial y} + \frac{\partial^2\psi}{\partial x^2}T^p_{11} - \frac{\partial^2\psi}{\partial y^2}T^p_{22} + \kappa T^p_{12}\left(T^p_{11} + T^p_{22}\right)\right) = \left(\frac{\partial^2\psi}{\partial y^2} - \frac{\partial^2\psi}{\partial x^2}\right). \tag{2.13}$$

In natural stress variables, these take the form

$$\frac{\lambda}{\mathrm{Wi}} + (\mathbf{v}.\nabla)\lambda + 2\mu\nabla.\mathbf{w} + \kappa\left(\left(\lambda|\mathbf{v}| - \frac{1}{\mathrm{Wi}|\mathbf{v}|}\right)^2 + \frac{\mu^2}{|\mathbf{v}|^2}\right) = \frac{1}{\mathrm{Wi}^2|\mathbf{v}|^2}, \tag{2.14}$$

$$\frac{\mu}{\mathrm{Wi}} + (\mathbf{v}.\nabla)\mu + \nu\nabla.\mathbf{w} + \kappa\left(\lambda|\mathbf{v}|^2 + \frac{\nu}{|\mathbf{v}|^2} - \frac{2}{\mathrm{Wi}}\right)\mu = 0, \tag{2.15}$$

$$\frac{\nu}{\mathrm{Wi}} + (\mathbf{v}.\nabla)\nu + \kappa\left(\left(\frac{\nu}{|\mathbf{v}|} - \frac{|\mathbf{v}|}{\mathrm{Wi}}\right)^2 + \mu^2|\mathbf{v}|^2\right) = \frac{|\mathbf{v}|^2}{\mathrm{Wi}^2}, \tag{2.16}$$

where, following the construction of Renardy [25, 26],

$$\mathbf{v} = (u, v)^T, \qquad \mathbf{w} = \left(-\frac{v}{u^2+v^2}, \frac{u}{u^2+v^2}\right)^T, \qquad \mathbf{T}^p + \frac{\mathbf{I}}{\mathrm{Wi}} = \lambda\mathbf{v}\mathbf{v}^T + \mu(\mathbf{v}\mathbf{w}^T + \mathbf{w}\mathbf{v}^T) + \nu\mathbf{w}\mathbf{w}^T. \tag{2.17}$$

3 Asymptotic analysis

In the limit $r \to 0$, as the singularity is approached, we obtain a three region structure. This is summarised in Figure 2. The outer or core region is presented first and then matched to boundary layers at the stick and slip surfaces. The boundary layer at the stick surface arises so that the polymer stress equations can accommodate viscometric behaviour. The boundary layer at the slip surface is necessary for the accommodation of finite elongational polymer stresses.

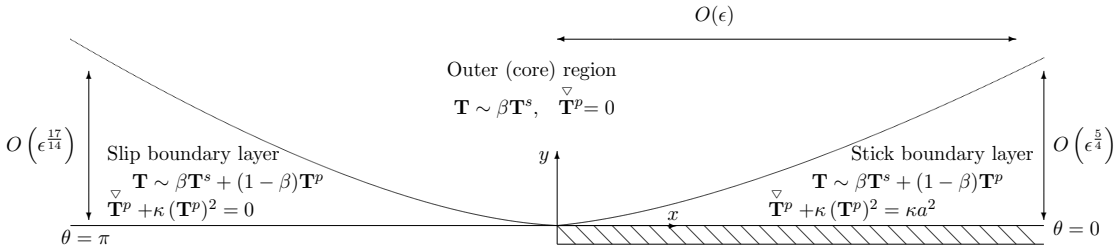

Slip boundary layer balances:

$\mathbf{v}\cdot\nabla\lambda + \kappa\lambda^2u^2 = 0$

$\mathbf{v}\cdot\nabla\mu + \kappa\lambda\mu u^2 = 0$

$\mathbf{v}\cdot\nabla\nu + \kappa\lambda u^2(\mu^2 - a^2) = 0$

with $a^2 = \dfrac{1-\kappa}{\kappa\mathrm{Wi}^2}$

Extra-stresses:

$T_{11} \sim \beta T^s_{11} + (1-\beta)T^p_{11}$

$T_{12} \sim \beta T^s_{12} + (1-\beta)T^p_{12}$

$T_{22} \sim \beta T^s_{22}$

Outer (core) flow:

$\mathbf{v}\cdot\nabla\lambda = 0$

$\mathbf{v}\cdot\nabla\mu = 0$

$\mathbf{v}\cdot\nabla\nu = 0$

$\mathbf{T}^s = O(\epsilon^{-\frac{1}{2}})$

$\mathbf{T}^p = O(\epsilon^{-\frac{5}{16}})$

Stick boundary layer balances:

$\mathbf{v}\cdot\nabla\lambda + 2\mu\nabla\cdot\mathbf{w} + \kappa\lambda^2u^2 = 0$

$\mathbf{v}\cdot\nabla\mu + \nu\nabla\cdot\mathbf{w} + \kappa\lambda\mu u^2 = 0$

$\mathbf{v}\cdot\nabla\nu + \kappa\lambda u^2(\mu^2 - a^2) = 0$

with $\nabla\cdot\mathbf{w} \sim \dfrac{\partial}{\partial y}\left(\dfrac{1}{u}\right)$, $a^2 = \dfrac{1-\kappa}{\kappa\mathrm{Wi}^2}$

Extra-stresses:

$T_{11} \sim \beta T^s_{11} + (1-\beta)T^p_{11}$

$T_{12} \sim \beta T^s_{12}, \quad T_{22} \sim \beta T^s_{22}$

Figure 2: Asymptotic structure local to the singularity. The scalings are shown in terms of the small parameter ϵ, which represents the horizontal and radial distances on which this structure holds.

3.1 The outer (core) solution

The outer region is designated as being near to the singularity, but away from the stick and slip surfaces. Thus radial distances are small $r \ll 1$ with $0 < \theta < \pi$. We verify *a posteriori* that the solvent stress dominates the polymer stress

$$(1-\beta)\mathbf{T}^p \ll \beta \mathbf{T}^s \qquad \text{as } r \to 0, \tag{3.1}$$

with both possessing singular behaviour. This gives the Newtonian balance $\mathbf{T} \sim \beta \mathbf{T}^s$ at leading order for the extra stress. The momentum equation reduces to the Stokes flow equation with the upper convective derivative of the polymer stress dominating in its constitutive equation, namely

$$0 = -\nabla p + \beta \nabla^2 \mathbf{v}, \qquad \overset{\triangledown}{\mathbf{T}}{}^p = 0. \tag{3.2}$$

A discussion on the separable self-similar solutions for Stokes flow for the edge condition at the singularity is given in Richardson [27], noting the reference to earlier work of Michael [22] and Moffatt [23]. The physically relevant dominant self-similar solution may be written as

$$\psi \sim 2\kappa C_0 r^{\frac{3}{2}} \sin\left(\frac{\theta}{2}\right) \sin\theta, \qquad p \sim 2\beta\kappa C_0 r^{-\frac{1}{2}} \sin\left(\frac{\theta}{2}\right), \qquad \text{as } r \to 0, \tag{3.3}$$

with the arbitrary constant C_0 being set by the flow away from the singularity. The sign of C_0 determines the flow direction with negative values occurring for stick-slip flows and positive values for slip-stick. The polymer stress equation in (3.2) has the stretching solution

$$\mathbf{T}^p + \frac{\mathbf{I}}{\mathrm{Wi}} \sim \lambda(\psi)\, \mathbf{v}\mathbf{v}^T, \qquad \lambda(\psi) = \frac{C_1}{\kappa^2 C_0^2} \left(\frac{\psi}{\kappa C_0}\right)^{-\frac{7}{8}} \qquad \text{as } r \to 0, \tag{3.4}$$

with C_1 an arbitrary constant. This leading order outer solution gives the estimates

$$\mathbf{v} = O(r^{\frac{1}{2}}), \qquad \nabla\mathbf{v} = O(r^{-\frac{1}{2}}), \qquad \mathbf{T}^s = O(r^{-\frac{1}{2}}) \qquad \mathbf{T}^p = O(r^{-\frac{5}{16}}) \qquad \text{as } r \to 0, \tag{3.5}$$

confirming the assumed dominant balances. The behaviour of the natural stress variables in this region, may be determined from (2.14)–(2.16), which at leading order are

$$(\mathbf{v}.\nabla)\lambda = 0, \qquad (\mathbf{v}.\nabla)\mu = 0, \qquad (\mathbf{v}.\nabla)\nu = 0. \tag{3.6}$$

The variables μ and ν are thus also constant along streamlines, with the forms

$$\mu = C_2, \qquad \nu = \kappa^2 C_0^2 C_3 \left(\frac{\psi}{\kappa C_0}\right)^{\frac{7}{8}}, \tag{3.7}$$

along with that for λ in (3.4) being determined by matching to the boundary layer at the stick surface (given in section 3.2). There are three free constants C_1, C_2, C_3 each associated with a natural stress variable, which communicate the necessary polymer stress information between the boundary layers at the stick and slip surfaces. The order of magnitude estimates

$$\lambda = O(r^{-\frac{21}{16}}), \qquad \mu = O(1), \qquad \nu = O(r^{\frac{21}{16}}), \tag{3.8}$$

may be used to confirm the dominance of the terms in (3.6) within the constitutive equations (2.14)–(2.16).

For the above outer solution we may determine the limiting behaviours as the stick and slip surfaces are approached. This is required for matching and may also be used to determine where changes in dominant balance occur leading to the required boundary layers. Approaching the stick surface, we have

$$\begin{aligned}
\text{as } y \to 0^+, x > 0, \qquad & \psi \sim \kappa C_0 x^{-\frac{1}{2}} y^2, \quad u \sim 2\kappa C_0 x^{-\frac{1}{2}} y, \quad v \sim \frac{1}{2}\kappa C_0 x^{-\frac{3}{2}} y^2, \\
& p \sim \beta\kappa C_0 x^{-\frac{3}{2}} y, \quad T_{11}^s = -T_{22}^s \sim -2\kappa C_0 x^{-\frac{3}{2}} y, \quad T_{12}^s \sim 2\kappa C_0 x^{-\frac{1}{2}}, \\
& T_{11}^p \sim 4C_1 x^{-\frac{9}{16}} y^{\frac{1}{4}}, \quad T_{12}^p \sim C_1 x^{-\frac{25}{16}} y^{\frac{5}{4}}, \quad T_{22}^p + \frac{1}{\mathrm{Wi}} \sim \frac{1}{4} C_1 x^{-\frac{41}{16}} y^{\frac{9}{4}}, \\
& \lambda \sim \frac{C_1}{\kappa^2 C_0^2} x^{\frac{7}{16}} y^{-\frac{7}{4}}, \quad \mu \sim C_2, \quad \nu \sim \kappa^2 C_0^2 C_3 x^{-\frac{7}{16}} y^{\frac{7}{4}}.
\end{aligned} \tag{3.9}$$

The polymer and solvent T_{11} components become the same size when $y = O(x^{\frac{5}{4}})$, which gives the scaling for the boundary layer thickness at the stick surface. For the slip surface we have

$$\begin{aligned}
\text{as } y \to 0^+, x < 0, \quad & \psi \sim 2\kappa C_0(-x)^{\frac{1}{2}} y + \frac{1}{4}\kappa C_0(-x)^{-3/2} y^3, \quad u \sim 2\kappa C_0(-x)^{\frac{1}{2}}, \quad v \sim \kappa C_0(-x)^{-\frac{1}{2}} y, \\
& p \sim 2\beta\kappa C_0(-x)^{-\frac{1}{2}}, \quad T_{11}^s = -T_{22}^s \sim -2\kappa C_0(-x)^{-\frac{1}{2}}, \quad T_{12}^s \sim 2\kappa C_0(-x)^{-\frac{3}{2}} y \\
& T_{11}^p \sim 4C_1(-x)^{\frac{9}{16}}(2y)^{-\frac{7}{8}}, \quad T_{12}^p \sim C_1(-x)^{-\frac{7}{16}}(2y)^{\frac{1}{8}}, \quad T_{22}^p + \frac{1}{\mathrm{Wi}} \sim \frac{1}{4}C_1(-x)^{-\frac{23}{16}}(2y)^{\frac{9}{8}}, \\
& \lambda \sim \frac{C_1}{\kappa^2 C_0^2}(-x)^{-\frac{7}{16}}(2y)^{-\frac{7}{8}} \quad \mu \sim C_2, \quad \nu \sim \kappa^2 C_0^2 C_3 (-x)^{\frac{7}{16}}(2y)^{\frac{7}{8}}. \qquad (3.10)
\end{aligned}$$

The polymer and solvent normal T_{11} and shear T_{12} stress components become the same size when $y = O((-x)^{\frac{17}{14}})$, which gives the scaling for the boundary layer at the slip surface.

3.2 Stick surface boundary layer

We represent the length scale on which the asymptotic analysis holds, through a small positive artificial parameter ϵ. The scalings for the boundary layer at the stick surface are then

$$x = \epsilon\bar{X}, \qquad y = \epsilon^{\frac{5}{4}}\bar{Y}, \qquad \psi = \epsilon^2\bar{\Psi}, \qquad u = \epsilon^{\frac{3}{4}}\bar{u}, \qquad v = \epsilon\bar{v}, \qquad p = \epsilon^{-\frac{1}{4}}\bar{p},$$

$$T_{11}^p = \epsilon^{-\frac{1}{4}}\bar{T}_{11}^p, \quad T_{12}^p = \bar{T}_{12}^p, \quad T_{22}^p = -\frac{1}{\mathrm{Wi}} + \epsilon^{\frac{1}{4}}\bar{T}_{22}^p, \quad T_{11}^s = \epsilon^{-\frac{1}{4}}\bar{T}_{11}^s, \quad T_{12}^s = \epsilon^{-\frac{1}{2}}\bar{T}_{12}^s, \quad T_{22}^s = \epsilon^{-\frac{1}{4}}\bar{T}_{22}^s,$$

$$\lambda = \epsilon^{-\frac{7}{4}}\bar{\lambda}, \qquad \mu = \bar{\mu}, \qquad \nu = \epsilon^{\frac{7}{4}}\bar{\nu}. \qquad (3.11)$$

as suggested by the limiting outer behaviours in (3.9) and dominant balance in the governing equations. The total extra stresses are thus

$$T_{11} = \epsilon^{-\frac{1}{4}}\left(\beta\bar{T}_{11}^s + (1-\beta)\bar{T}_{11}^p\right), \quad T_{12} = \epsilon^{-\frac{1}{2}}\left(\beta\bar{T}_{12}^s + \epsilon^{\frac{1}{2}}(1-\beta)\bar{T}_{12}^p\right),$$

$$T_{22} = \epsilon^{-\frac{1}{4}}\left(\beta\bar{T}_{22}^s - \epsilon^{\frac{1}{4}}\frac{(1-\beta)}{\mathrm{Wi}} + \epsilon^{\frac{1}{2}}(1-\beta)\bar{T}_{22}^p\right),$$

illustrating that it is only the normal T_{11} stress components that balance in this boundary layer region, the other polymer stress components being subdominant to their solvent counterparts. For the region $\bar{X} > 0, \bar{Y} = O(1)$ we have the leading order momentum equations

$$\begin{aligned}
0 &= \beta\frac{\partial^3\bar{\Psi}}{\partial\bar{Y}^3} + \epsilon^{\frac{1}{2}}\left(-\frac{\partial\bar{p}}{\partial\bar{X}} + \beta\frac{\partial^3\bar{\Psi}}{\partial\bar{X}^2\partial\bar{Y}} + (1-\beta)\frac{\partial\bar{T}_{11}^p}{\partial\bar{X}} + (1-\beta)\frac{\partial\bar{T}_{12}^p}{\partial\bar{Y}}\right), \\
0 &= -\frac{\partial\bar{p}}{\partial\bar{Y}} - \beta\frac{\partial^3\bar{\Psi}}{\partial\bar{X}\partial\bar{Y}^2} + \epsilon^{\frac{1}{2}}\left(-\beta\frac{\partial^3\bar{\Psi}}{\partial\bar{X}^3} + (1-\beta)\frac{\partial\bar{T}_{12}^p}{\partial\bar{X}} + (1-\beta)\frac{\partial\bar{T}_{22}^p}{\partial\bar{Y}}\right).
\end{aligned}$$

Thus the stream function and solvent stresses are unchanged at leading order through this boundary layer with explicit solution

$$\bar{\Psi} = \kappa C_0\bar{X}^{-\frac{1}{2}}\bar{Y}^2, \quad \bar{T}_{11}^s = -\bar{T}_{22}^s = -2\beta\kappa C_0\bar{X}^{-\frac{3}{2}}\bar{Y}, \quad \bar{T}_{12}^s = 2\beta\kappa C_0\bar{X}^{-\frac{1}{2}}, \qquad (3.12)$$

where we have used the matching conditions (3.9). The pressure is given by

$$\bar{p} = \beta\kappa C_0\bar{X}^{-\frac{3}{2}}\bar{Y} + p_0\bar{X}^{-\frac{1}{4}},$$

where the additive function of $\bar{X}$ with constant p_0 is suggested by scaling.

Using the scalings (3.11) in (2.11)–(2.13), the leading order polymer stresses satisfy the boundary layer equations

$$\left(\frac{\partial\bar\Psi}{\partial\bar Y}\frac{\partial\bar T^p_{11}}{\partial\bar X}-\frac{\partial\bar\Psi}{\partial\bar X}\frac{\partial\bar T^p_{11}}{\partial\bar Y}-2\frac{\partial^2\bar\Psi}{\partial\bar X\partial\bar Y}\bar T^p_{11}-2\frac{\partial^2\bar\Psi}{\partial\bar Y^2}\bar T^p_{12}\right)+\kappa\bar T^{p2}_{11}=0, \tag{3.13}$$

$$\left(\frac{\partial\bar\Psi}{\partial\bar Y}\frac{\partial\bar T^p_{22}}{\partial\bar X}-\frac{\partial\bar\Psi}{\partial\bar X}\frac{\partial\bar T^p_{22}}{\partial\bar Y}+2\frac{\partial^2\bar\Psi}{\partial\bar X\partial\bar Y}\bar T^p_{22}+2\frac{\partial^2\bar\Psi}{\partial\bar X^2}\bar T^p_{12}\right)+\kappa\bar T^{p2}_{12}=\frac{1-\kappa}{\mathrm{Wi}^2}, \tag{3.14}$$

$$\left(\frac{\partial\bar\Psi}{\partial\bar Y}\frac{\partial\bar T^p_{12}}{\partial\bar X}-\frac{\partial\bar\Psi}{\partial\bar X}\frac{\partial\bar T^p_{12}}{\partial\bar Y}+\frac{\partial^2\bar\Psi}{\partial\bar X^2}\bar T^p_{11}-\frac{\partial^2\bar\Psi}{\partial\bar Y^2}\bar T^p_{22}\right)+\kappa\bar T^p_{12}\bar T^p_{11}=0. \tag{3.15}$$

These equations are the high Weissenberg number boundary layer equations of Hagen and Renardy [15], which seem to manifest themselves at solid surfaces in the neighbourhood of singularities even in Weissenberg $O(1)$ flows. The re-entrant corner singularity described in [7] being another example. We impose on these equations the matching conditions

$$\text{as } \bar Y\to+\infty,\qquad \bar T^p_{11}\sim 4C_1\bar X^{-\frac{9}{16}}\bar Y^{\frac14},\quad \bar T^p_{12}\sim C_1\bar X^{-\frac{25}{16}}\bar Y^{\frac54},\quad \bar T^p_{22}\sim\frac14 C_1\bar X^{-\frac{41}{16}}\bar Y^{\frac94}, \tag{3.16}$$

as well as the viscometric wall stress behaviour

$$\text{as } \bar Y\to0^+,\qquad \bar T^p_{11}\sim 2a^{\frac12}|C_0|^{\frac12}\bar X^{-\frac14},\quad \bar T^p_{12}\sim aC_0|C_0|^{-1},\quad \bar T^p_{22}\sim a^{\frac32}|C_0|^{-\frac12}\bar X^{\frac14}. \tag{3.17}$$

Here we have conveniently introduced the parameter

$$a=\frac{1}{\mathrm{Wi}}\left(\frac{1-\kappa}{\kappa}\right)^{\frac12}. \tag{3.18}$$

For definiteness, we take $a>0$ and it is necessarily real since $0<\kappa<1$.

The polymer stress boundary layer equations (3.13)–(3.15) have the similarity solution

$$\xi=a^{-\frac12}|C_0|^{\frac12}\frac{\bar Y}{\bar X^{\frac54}},\qquad \bar\Psi=a\kappa C_0|C_0|^{-1}\bar X^2\xi^2,$$

$$\bar T^p_{11}=a^{\frac12}|C_0|^{\frac12}\bar X^{-\frac14}t^p_{11}(\xi),\qquad \bar T^p_{12}=at^p_{12}(\xi),\qquad \bar T^p_{22}=a^{\frac32}|C_0|^{-\frac12}\bar X^{\frac14}t^p_{22}(\xi), \tag{3.19}$$

where we have taken the opportunity to scale out both the free parameter C_0 and combined parameter a. We thus obtain

$$2\xi^2{t^p_{11}}'-\frac32\xi t^p_{11}+4t^p_{12}\pm(t^p_{11})^2=0, \tag{3.20}$$

$$2\xi^2{t^p_{22}}'-\frac32\xi^2 t^p_{12}+\frac32\xi t^p_{22}\pm((t^p_{12})^2-1)=0, \tag{3.21}$$

$$2\xi^2{t^p_{12}}'-\frac34\xi^2 t^p_{11}+2t^p_{22}\pm t^p_{11}t^p_{12}=0, \tag{3.22}$$

$$\text{as } \xi\to0^+,\qquad t^p_{11}\sim2,\quad t^p_{12}\sim\mp1,\quad t^p_{22}\sim1, \tag{3.23}$$

$$\text{as } \xi\to+\infty,\qquad t^p_{11}\sim4C^*_1\xi^{\frac14},\quad t^p_{12}\sim C^*_1\xi^{\frac54},\quad t^p_{22}\sim\frac14C^*_1\xi^{\frac94}, \tag{3.24}$$

where $'$ denotes $d/d\xi$ and

$$C^*_1=C_1|C_0|^{-\frac58}a^{-\frac38}. \tag{3.25}$$

The equations (3.20)–(3.23) conveniently cover both flow direction situations, with the choice of upper sign for the stick-slip case $C_0<0$ and lower sign the slip-stick case $C_0>0$.

In natural stress variables, the analogous statement for the boundary layer equations (3.13)–(3.15) with imposed wall and outer matching conditions is

$$(\bar{\mathbf{v}}.\bar{\nabla})\bar{\lambda} + 2\bar{\mu}\frac{\partial}{\partial\bar{Y}}\left(\frac{1}{\bar{u}}\right) + \kappa\bar{\lambda}^2\bar{u}^2 = 0, \tag{3.26}$$

$$(\bar{\mathbf{v}}.\bar{\nabla})\bar{\mu} + \bar{\nu}\frac{\partial}{\partial\bar{Y}}\left(\frac{1}{\bar{u}}\right) + \kappa\bar{\lambda}\bar{\mu}\bar{u}^2 = 0, \tag{3.27}$$

$$(\bar{\mathbf{v}}.\bar{\nabla})\bar{\nu} + \kappa\bar{u}^2\left(\bar{\mu}^2 - a^2\right) = 0, \tag{3.28}$$

$$\text{as } \bar{Y}\to 0 \qquad \bar{\lambda} \sim \frac{a^{\frac{1}{2}}}{2\kappa^2}|C_0|^{-\frac{3}{2}}\bar{X}^{\frac{3}{4}}\bar{Y}^{-2}, \quad \bar{\mu} \sim aC_0|C_0|^{-1}, \quad \bar{\nu} \sim 4a^{\frac{3}{2}}\kappa^2|C_0|^{\frac{3}{2}}\bar{X}^{-\frac{3}{4}}\bar{Y}^2, \tag{3.29}$$

$$\text{as } \bar{Y}\to\infty \qquad \bar{\lambda} \sim \frac{C_1}{\kappa^2 C_0^2}\bar{X}^{\frac{7}{16}}\bar{Y}^{-\frac{7}{4}}, \quad \bar{\mu} \sim C_2, \quad \bar{\nu} \sim \kappa^2 C_0^2 C_3 \bar{X}^{-\frac{7}{16}}\bar{Y}^{\frac{7}{4}}. \tag{3.30}$$

The equations (3.26)–(3.28) follow immediately from (2.14)–(2.16), or can be deduced using

$$\bar{T}^p_{11} = \bar{\lambda}\bar{u}^2, \qquad \bar{T}^p_{12} = \bar{\lambda}\bar{u}\bar{v} + \bar{\mu}, \qquad \bar{T}^p_{22} = \bar{\lambda}\bar{v}^2 + 2\bar{\mu}\frac{\bar{v}}{\bar{u}} + \frac{\bar{\nu}}{\bar{u}^2}, \tag{3.31}$$

in (3.13)–(3.15). The relationships (3.31) link the two formulations, which follow at leading order in ϵ from introducing (3.11) into (2.17). In self-similar form with

$$\bar{\lambda} = \frac{|C_0|^{-\frac{1}{2}}}{a^{\frac{1}{2}}\kappa^2}\bar{X}^{-\frac{7}{4}}\tilde{\lambda}(\xi), \qquad \bar{\mu} = a\tilde{\mu}(\xi), \qquad \bar{\nu} = a^{\frac{5}{2}}\kappa^2|C_0|^{\frac{1}{2}}\bar{X}^{\frac{7}{4}}\tilde{\nu}(\xi),$$

the boundary layer equations, wall and far-field behaviours are

$$2\xi^2\tilde{\lambda}' + \frac{7}{2}\xi\tilde{\lambda} + \frac{\tilde{\mu}}{\xi^2} \pm 4\xi^2\tilde{\lambda}^2 = 0, \tag{3.32}$$

$$2\xi^2\tilde{\mu}' + \frac{\tilde{\nu}}{2\xi^2} \pm 4\xi^2\tilde{\lambda}\tilde{\mu} = 0, \tag{3.33}$$

$$2\xi^2\tilde{\nu}' - \frac{7}{2}\xi\tilde{\nu} \pm 4\xi^2(\tilde{\mu}^2 - 1) = 0, \tag{3.34}$$

$$\text{as } \xi\to 0^+ \qquad \tilde{\lambda} \sim \frac{1}{2\xi^2}, \quad \tilde{\mu} \sim \mp 1, \quad \tilde{\nu} \sim 4\xi^2, \tag{3.35}$$

$$\text{as } \xi\to+\infty \qquad \tilde{\lambda} \sim C_1^*\xi^{-\frac{7}{4}}, \quad \tilde{\mu} \sim C_2^*, \quad \tilde{\nu} \sim C_3^*\xi^{\frac{7}{4}}, \tag{3.36}$$

introducing the far-field similarity parameters

$$C_2^* = \frac{C_2}{a}, \qquad C_3^* = C_3|C_0|^{\frac{5}{8}}a^{-\frac{13}{8}}, \tag{3.37}$$

in addition to (3.25). As for (3.20)–(3.23), the upper sign choice corresponds to the stick-slip case $C_0 < 0$ and lower sign the slip-stick case $C_0 > 0$. The relationships (3.31) in similarity form are

$$t^p_{11} = 4\xi^2\tilde{\lambda}, \qquad t^p_{12} = \xi^3\tilde{\lambda} + \tilde{\mu}, \qquad t^p_{22} = \frac{1}{4}\xi^4\tilde{\lambda} + \frac{1}{2}\xi\tilde{\mu} + \frac{\tilde{\nu}}{4\xi^2}, \tag{3.38}$$

which link the Cartesian formulation (3.20)–(3.22) with (3.32)–(3.34). These suggest that the leading order far-field behaviour (3.24) in the Cartesian statement can be replaced with the more accurate expressions

$$t^p_{11} \sim 4C_1^*\xi^{\frac{1}{4}}, \qquad t^p_{12} \sim C_1^*\xi^{\frac{5}{4}} + C_2^*, \qquad t^p_{22} \sim \frac{1}{4}C_1^*\xi^{\frac{9}{4}} + \frac{1}{2}C_2^*\xi + \frac{1}{4}C_3^*\xi^{-\frac{1}{4}} \qquad \text{as } \xi\to\infty. \tag{3.39}$$

We first discuss numerical solutions for the stick-slip case $C_0 < 0$. The Cartesian (3.20)–(3.24) and natural stress (3.32)–(3.36) systems can be solved as initial value problems using the wall viscometric

behaviour as initial data posed at small ξ values. The systems were implemented in MATLAB [21] using the solver ode15s, tight error tolerances AbsTol=RelTol=10^{-13} and domain $[\xi_0, \xi_\infty]$ with $\xi_0 = 10^{-6}$ and $\xi_\infty = 10^{10}$. [1] Figure 3 shows the Cartesian profiles, all three stress components giving consistent estimates of the far-field constant C_1^* at stated in the caption of Figure 3. This agrees with the value obtained using natural stress variables stated below in (3.46). In principle, (3.39) could be used to determine the other two constants. However, it is difficult to obtain reliable estimates for these from the numerical scheme, even with the tight error tolerances used.

For the natural stress formulation, it is convenient to use the scaled variables

$$\ell(\xi) = \xi^2 \tilde{\lambda}, \qquad m(\xi) = \tilde{\mu}, \qquad n(\xi) = \frac{\tilde{\nu}}{\xi^2}, \tag{3.40}$$

for which (3.32)–(3.36) become

$$2\xi^2 \ell' - \frac{\xi \ell}{2} + m + 4\ell^2 = 0, \tag{3.41}$$

$$2\xi^2 m' + \frac{n}{2} + 4\ell m = 0, \tag{3.42}$$

$$2\xi^2 n' + \frac{\xi n}{2} + 4(m^2 - 1) = 0, \tag{3.43}$$

$$\text{at } \xi = \xi_0 \qquad \ell = \frac{1}{2}, \quad m = -1, \quad n = 4, \tag{3.44}$$

$$\text{at } \xi = \xi_\infty \qquad \ell = C_1^* \xi^{\frac{1}{4}}, \quad m = C_2^*, \quad n = C_3^* \xi^{-\frac{1}{4}}. \tag{3.45}$$

Figure 4 shows the profiles and convergence to the far-field behaviours, which give the estimates

$$C_1^* = 0.3337128..., \qquad C_2^* = -0.6681786..., \qquad C_3^* = 4.3344536.... \tag{3.46}$$

These values are sensitive to the initial starting point. As an illustration of their accuracy, taking $\xi_0 = 10^{-7}$ affects the 6th d.p. of C_1^* and the 4th d.p. in C_2^* and C_3^*.

For the slip-stick case, flow direction is reversed with now $C_0 > 0$ and the lower sign choice taken. The Cartesian (3.20)–(3.24) and natural stress (3.32)–(3.36) systems are again to be solved as initial value problems, but now using the far-field behaviour as initial data. The wall viscometric behaviour is to be obtained. In principle the Cartesian equations can be used, provided the far-field behaviour (3.39) is used. However, we present results only for the natural stress equations. For slip-stick, (3.32)–(3.36) are

$$2\xi^2 \ell' - \frac{\xi \ell}{2} + m - 4\ell^2 = 0, \tag{3.47}$$

$$2\xi^2 m' + \frac{n}{2} - 4\ell m = 0, \tag{3.48}$$

$$2\xi^2 n' + \frac{\xi n}{2} - 4(m^2 - 1) = 0, \tag{3.49}$$

$$\text{at } \xi = \xi_\infty \qquad \ell = C_1^* \xi^{\frac{1}{4}}, \quad m = C_2^*, \quad n = C_3^* \xi^{-\frac{1}{4}}. \tag{3.50}$$

$$\text{at } \xi = \xi_0 \qquad \ell = \frac{1}{2}, \quad m = 1, \quad n = 4, \tag{3.51}$$

These equations were implemented in MATLAB as for the above stick-slip case, with the same domain and error tolerances, but now with (3.50) used as initial data. The far-field constants are supplied by stresses from the slip layer. As base values we consider those form the stick-slip case in (3.46), allowing for appropriate changes in sign. The value of C_1^* is expected to be negative, to avoid singular behaviour

[1] The solver ode15s is variable order based on numerical differentiation formulas and is slightly more accurate in this problem than the explicit Runge-Kutta solver ode45. The tolerances have been set to their minimum to increase accuracy for the far-field parameter estimates. The interval end points ξ_0 and ξ_∞ are chosen as small and as large as possible to minimise the perturbation terms to the asymptotic expressions in (3.23) and (3.24).

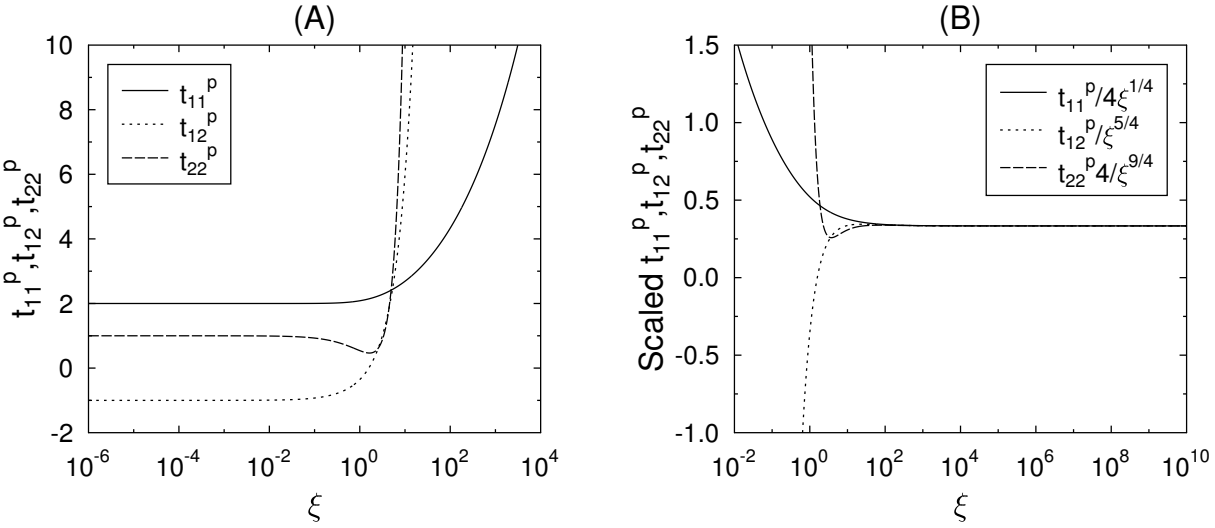

Figure 3: Stick-slip problem Cartesian variables. Illustration of the numerical solution to (3.20)–(3.22) as an initial value problem with (3.23) posed at $\xi = \xi_0 = 10^{-6}$. (A) gives the profiles, whilst (B) shows convergence to the far-field behaviour (3.24). All three stress variables give consistent estimates of the parameter $C_1^* = 0.3337128....$

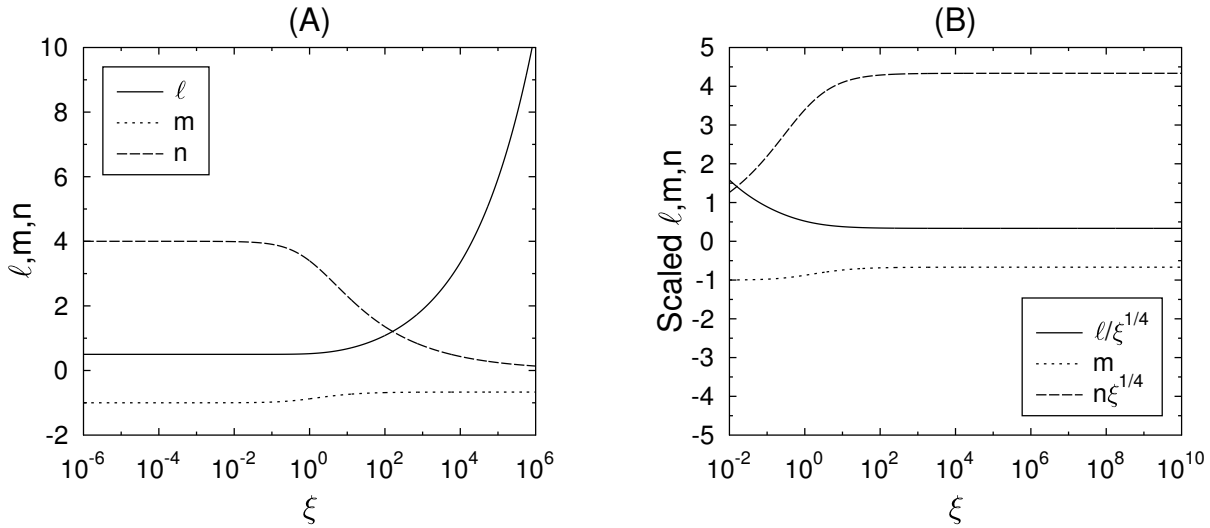

Figure 4: Stick-slip problem natural stress variables. Numerical solution to (3.41)–(3.43) as an initial value problem, with (3.44) posed as initial data at $\xi = \xi_0 = 10^{-6}$. (A) gives the profiles, whilst (B) shows convergence to the far-field behaviour (3.45). Estimates of the far-field parameters are given in (3.46).

within the slip layer. Shown in Figure 5 are profiles for selected values of the far-field constants covering the four possible sign combinations for C_2^* and C_3^* when $C_1^* < 0$. The profiles in Figure 5 (A) and (B) have far-field constants similar in magnitude to the base values in (3.46). Convergence to the wall behaviour could not be obtained when $C_2^* < 0$ in (C) and (D) without reducing the size of the values as stated. Shown in Figure 6 are the profiles for the various sign combinations when the base values are each divided by a factor of 10. This choice is arbitrary and chosen for purely illustrative reasons. It is noteworthy, that the oscillatory behaviour of the polymer stresses is significantly reduced. In the slip-stick regime, the slip layer would be expected to supply a range of values for the far-field constants. However, we omit a full parameter investigation of the solution dependence on the far-field constants, our purpose being to illustrate numerically solutions to the stick boundary layer equations.

A remark worth making for the Giesekus equations is the sign choice for viscometric behaviour. The boundary layer equations (3.13)–(3.15) possess the behaviour

$$\text{as } Y \to 0^+ \qquad (\bar{T}_{12}^p)^2 \sim a^2, \quad (\bar{T}_{11}^p)^2 \sim \frac{2}{\kappa}\frac{\partial^2 \bar{\Psi}}{\partial \bar{Y}^2}\bar{T}_{12}^p, \quad \bar{T}_{22}^p \sim \frac{2a^2}{\bar{T}_{11}^p}. \tag{3.52}$$

As such, there is a sign choice for $\bar{T}_{11}^p$, where in (3.17) we have adopted the positive root for $\bar{T}_{11}^p$ (and hence $\bar{T}_{22}^p$). Equally, there is at least mathematically the possibility of the negative root, with appropriate sign change for the natural stress variables. However, it is interesting to note that the numerical results in Figures 5 and 6 always seem to choose the positive root. The choice of sign for $\bar{T}_{12}^p$ is dictated by that of $\frac{\partial^2 \bar{\Psi}}{\partial \bar{Y}^2} = 2\kappa C_0 \bar{X}^{-\frac{1}{2}}$ and hence the sign of C_0 (i.e. the flow direction) for which there is no ambiguity.

3.3 Slip surface boundary layer

The boundary layer variables at the slip surface are given by the scalings

$$x = \epsilon \bar{X}, \qquad y = \epsilon^{\frac{17}{14}} \bar{Y}, \qquad \psi = \epsilon^{\frac{12}{7}} \bar{\Psi}, \qquad u = \epsilon^{\frac{1}{2}} \bar{u}, \qquad v = \epsilon^{\frac{5}{7}} \bar{v}, \qquad p = \epsilon^{-\frac{1}{2}} \bar{p},$$

$$T_{11}^p = \epsilon^{-\frac{1}{2}} \bar{T}_{11}^p, \quad T_{12}^p = \epsilon^{-\frac{2}{7}} \bar{T}_{12}^p, \quad T_{22}^p = \epsilon^{-\frac{1}{14}} \bar{T}_{22}^p, \quad T_{11}^s = \epsilon^{-\frac{1}{2}} \bar{T}_{11}^s, \quad T_{12}^s = \epsilon^{-\frac{2}{7}} \bar{T}_{12}^s, \quad T_{22}^s = \epsilon^{-\frac{1}{2}} \bar{T}_{22}^s.$$

$$\lambda = \epsilon^{-\frac{3}{2}} \bar{\lambda}, \qquad \mu = \bar{\mu}, \qquad \nu = \epsilon^{\frac{3}{2}} \bar{\nu}, \tag{3.53}$$

where $x < 0$ and $\epsilon > 0$ an artificial small parameter. These follow from (3.10) and recovering the quadratic stress terms in the constitutive equations. At the slip surface, the flow is expected to be strongly elongational, so balance of the upper convective stress derivative and quadratic stress terms would be anticipated physically. In $\bar{X} < 0, \bar{Y} = O(1)$ we then have the momentum equations

$$0 = \beta \frac{\partial^3 \bar{\Psi}}{\partial \bar{Y}^3} + \epsilon^{\frac{3}{7}} \left(-\frac{\partial \bar{p}}{\partial \bar{X}} + \beta \frac{\partial^3 \bar{\Psi}}{\partial \bar{X}^2 \partial \bar{Y}} + (1-\beta)\frac{\partial \bar{T}_{11}^p}{\partial \bar{X}} + (1-\beta)\frac{\partial \bar{T}_{12}^p}{\partial \bar{Y}} \right),$$

$$0 = -\frac{\partial \bar{p}}{\partial \bar{Y}} - \beta \frac{\partial^3 \bar{\Psi}}{\partial \bar{X} \partial \bar{Y}^2} + \epsilon^{\frac{3}{7}} \left(-\beta \frac{\partial^3 \bar{\Psi}}{\partial \bar{X}^3} + (1-\beta)\frac{\partial \bar{T}_{12}^p}{\partial \bar{X}} + (1-\beta)\frac{\partial \bar{T}_{22}^p}{\partial \bar{Y}} \right).$$

Thus the stream function and pressure are unchanged at leading order through this boundary layer with explicit solution

$$\bar{\Psi} = 2\kappa C_0 (-\bar{X})^{\frac{1}{2}} \bar{Y}, \quad \bar{p} = 2\beta\kappa C_0 (-\bar{X})^{-\frac{1}{2}}. \tag{3.54}$$

The leading order normal solvent stresses are unchanged, namely

$$\bar{T}_{11}^s = -\bar{T}_{22}^s = -2\kappa C_0 (-\bar{X})^{-\frac{1}{2}}, \tag{3.55}$$

and match with (3.10). However, the next term in the stream function expansion is required to calculate the solvent shear stress, which can be determined once the leading order polymer stresses are obtained. Nevertheless, the scalings for the extra stresses in this region are

$$T_{11} = \epsilon^{-\frac{1}{2}} \left(\beta \bar{T}_{11}^s + (1-\beta)\bar{T}_{11}^p \right), \quad T_{12} = \epsilon^{-\frac{2}{7}} \left(\beta \bar{T}_{12}^s + (1-\beta)\bar{T}_{12}^p \right), \quad T_{22} = \epsilon^{-\frac{1}{2}} \left(\beta \bar{T}_{22}^s + \epsilon^{\frac{3}{10}}(1-\beta)\bar{T}_{22}^p \right),$$

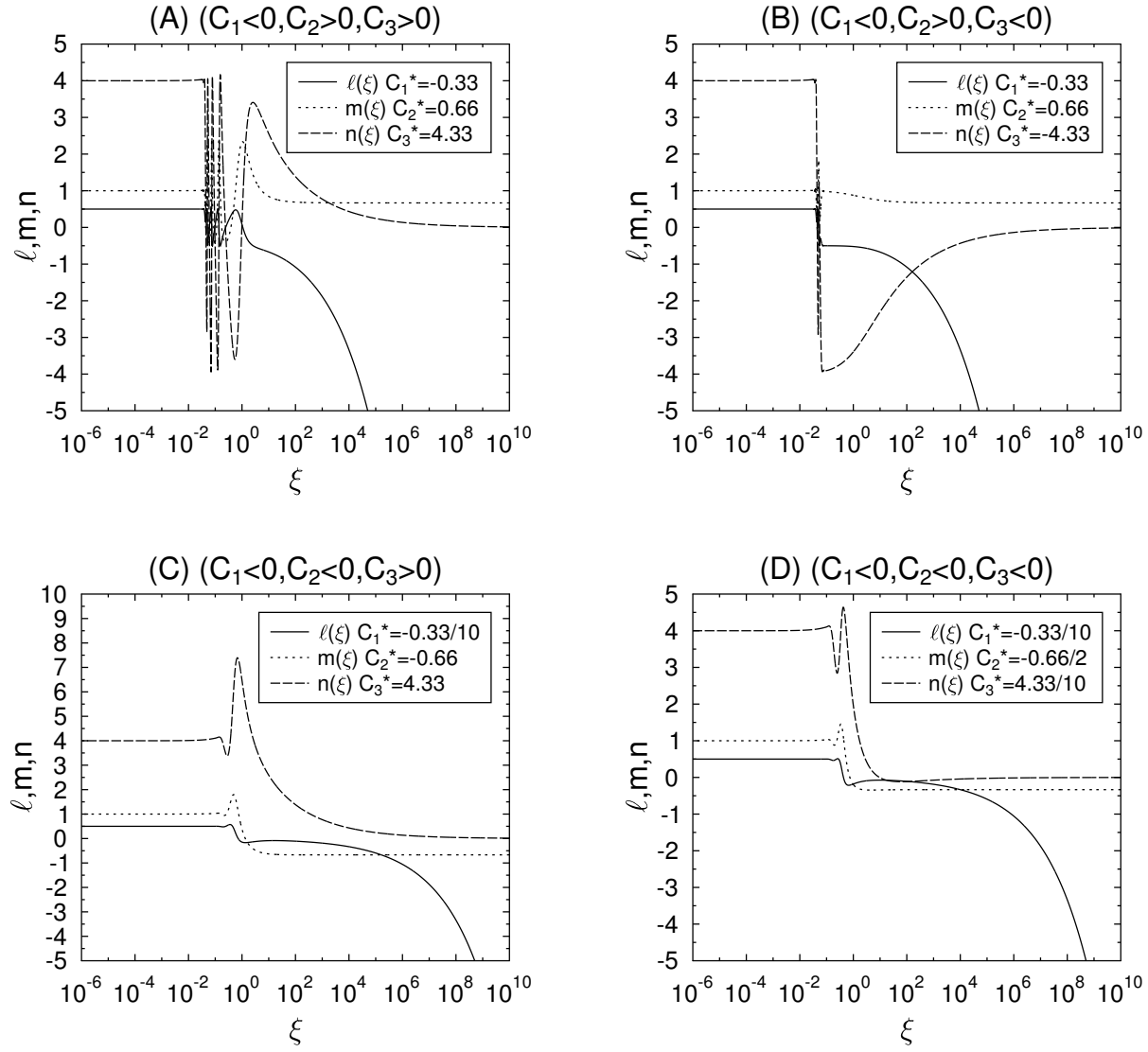

Figure 5: Slip-stick problem. Numerical solution to (3.47)–(3.48) with initial data (3.50). Far-field constants are as stated with $C_1^* < 0$ and different sign combinations for C_2^* and C_3^*.

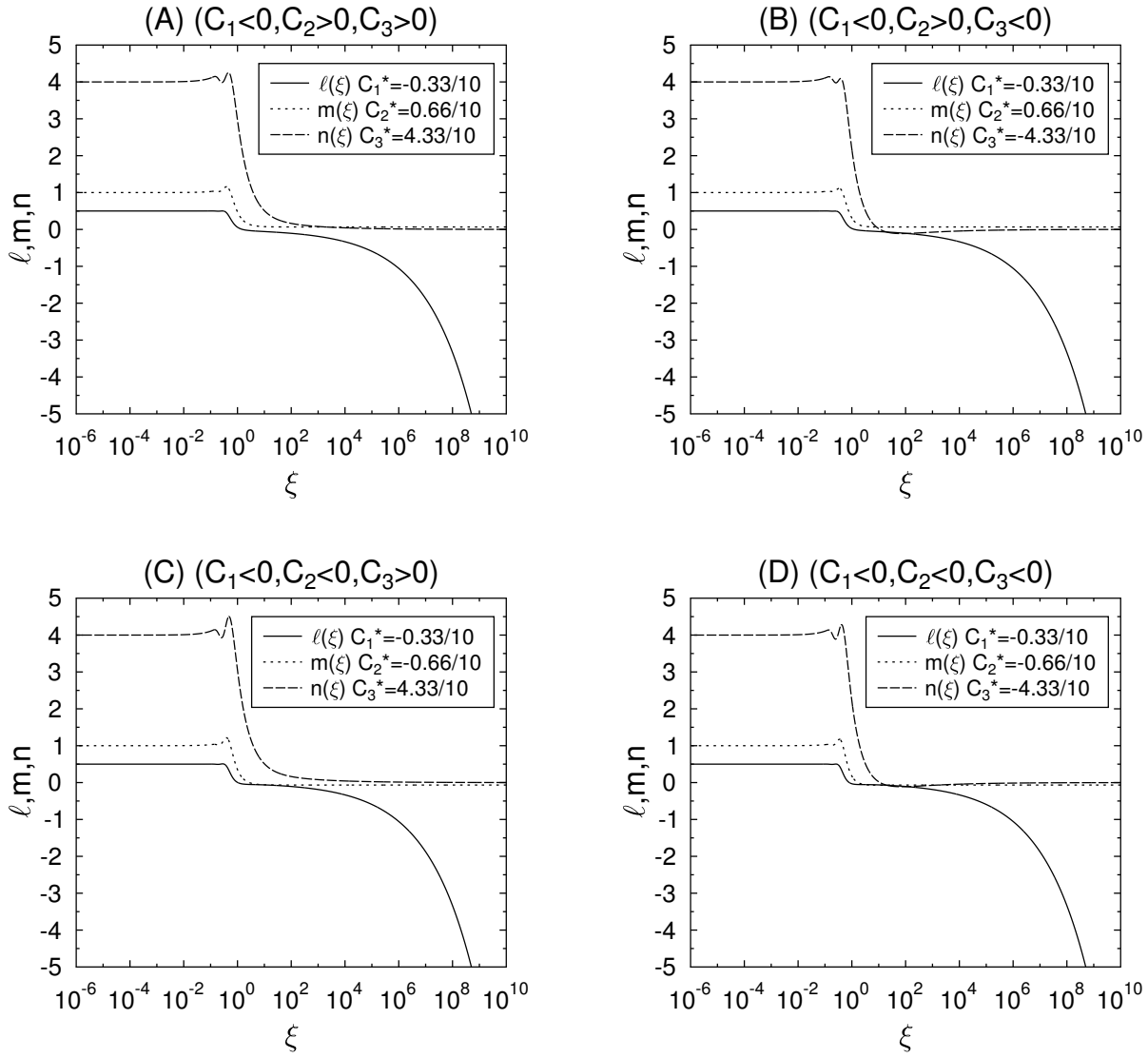

Figure 6: Slip-stick problem. Corresponding profiles to the cases in Figure 5, but for smaller far-field constants. The constants have been reduced by a factor of 10 from the magnitudes obtained in the stick-slip case.

where it is worth noting that both the solvent and polymer normal T_{11} and shear stresses are comparable. Writing $T_{12} = \epsilon^{-\frac{2}{7}}\bar{T}_{12}$, the leading order total shear stress can be obtained directly from the momentum equation to give

$$\bar{T}_{12} = 2\beta\kappa C_0(-\bar{X})^{-\frac{3}{2}}\bar{Y} - (1-\beta)\int_0^{\bar{Y}} \frac{\partial \bar{T}^p_{11}(\bar{X},Z)}{\partial \bar{X}}dZ, \tag{3.56}$$

after imposing the no shear stress condition on the slip surface $\bar{Y} = 0$.

The polymer stress boundary layer equations are

$$\left(\frac{\partial\bar{\Psi}}{\partial\bar{Y}}\frac{\partial\bar{T}^p_{11}}{\partial\bar{X}} - \frac{\partial\bar{\Psi}}{\partial\bar{X}}\frac{\partial\bar{T}^p_{11}}{\partial\bar{Y}} - 2\frac{\partial^2\bar{\Psi}}{\partial\bar{X}\partial\bar{Y}}\bar{T}^p_{11} - 2\frac{\partial^2\bar{\Psi}}{\partial\bar{Y}^2}\bar{T}^p_{12}\right) + \kappa\bar{T}^{p2}_{11} = 0, \tag{3.57}$$

$$\left(\frac{\partial\bar{\Psi}}{\partial\bar{Y}}\frac{\partial\bar{T}^p_{22}}{\partial\bar{X}} - \frac{\partial\bar{\Psi}}{\partial\bar{X}}\frac{\partial\bar{T}^p_{22}}{\partial\bar{Y}} + 2\frac{\partial^2\bar{\Psi}}{\partial\bar{X}\partial\bar{Y}}\bar{T}^p_{22} + 2\frac{\partial^2\bar{\Psi}}{\partial\bar{X}^2}\bar{T}^p_{12}\right) + \kappa\bar{T}^{p2}_{12} = 0, \tag{3.58}$$

$$\left(\frac{\partial\bar{\Psi}}{\partial\bar{Y}}\frac{\partial\bar{T}^p_{12}}{\partial\bar{X}} - \frac{\partial\bar{\Psi}}{\partial\bar{X}}\frac{\partial\bar{T}^p_{12}}{\partial\bar{Y}} + \frac{\partial^2\bar{\Psi}}{\partial\bar{X}^2}\bar{T}^p_{11} - \frac{\partial^2\bar{\Psi}}{\partial\bar{Y}^2}\bar{T}^p_{22}\right) + \kappa\bar{T}^p_{12}\bar{T}^p_{11} = 0, \tag{3.59}$$

and are subject to the matching conditions

$$\text{as } \bar{Y}\to+\infty, \quad T^p_{11} \sim 4C_1(-\bar{X})^{\frac{9}{16}}(2\bar{Y})^{-\frac{7}{8}}, \quad T^p_{12} \sim C_1(-\bar{X})^{-\frac{7}{16}}(2\bar{Y})^{\frac{1}{8}}, \quad T^p_{22} \sim \frac{1}{4}C_1(-\bar{X})^{-\frac{23}{16}}(2\bar{Y})^{\frac{9}{8}}. \tag{3.60}$$

For the stream function as given in (3.54), these equations have the exact solution

$$\bar{T}^p_{11} = (-C_0)(-\bar{X})^{-\frac{1}{2}}t^p_{11}(\xi), \quad \bar{T}^p_{12} = (-C_0)(-\bar{X})^{-\frac{2}{7}}t^p_{12}(\xi), \quad \bar{T}^p_{22} = (-C_0)(-\bar{X})^{-\frac{1}{14}}t^p_{22}(\xi), \tag{3.61}$$

where

$$\xi = \frac{2\bar{Y}}{(-\bar{X})^{\frac{17}{14}}}, \qquad t^p_{11} = \frac{3}{\left(1+3K_1\xi^{\frac{7}{8}}\right)}, \qquad t^p_{12} = \left(\frac{\xi}{4} + K_2\xi^{\frac{17}{24}}\right)t^p_{11},$$

$$t^p_{22} = \left(\frac{\xi^2}{16} + \frac{K_2}{2}\xi^{\frac{41}{24}} - \frac{K_2^2}{3K_1}\xi^{\frac{13}{24}}\right)t^p_{11} + K_3\xi^{\frac{13}{24}}, \tag{3.62}$$

for arbitrary constants K_1, K_2, K_3. The condition (3.60) determines

$$K_1 = \frac{-C_0}{4C_1}. \tag{3.63}$$

The other two constants are taken to be $K_2 = K_3 = 0$, as suggested below using natural stress variables. The relevant solution is thus

$$\bar{T}^p_{11} = \frac{-12C_0C_1(-\bar{X})^{\frac{9}{16}}}{\left(4C_1(-\bar{X})^{\frac{17}{16}} - 3C_0(2\bar{Y})^{\frac{7}{8}}\right)}, \quad \bar{T}^p_{12} = \frac{1}{2}(-\bar{X})^{-1}\bar{Y}\bar{T}^p_{11}, \quad \bar{T}^p_{22} = \frac{1}{4}(-\bar{X})^{-2}\bar{Y}^2\bar{T}^p_{11}. \tag{3.64}$$

On the slip surface $\bar{Y} = 0$, we have $\bar{T}^p_{11} = -3C_0(-\bar{X})^{-\frac{1}{2}}, \bar{T}^p_{12} = \bar{T}^p_{22} = 0$. This behaviour is the same as for linear PTT, the two constituent equations behaving similarly. It recovers the behaviour quoted in Tanner and Huang [35], who deduced this behaviour on the slip surface directly from the linear PTT equations assuming elongational flow in a Newtonian velocity field.

The natural stress statement for the polymer stress boundary layer equations is

$$(\bar{\mathbf{v}}.\bar{\nabla})\bar{\lambda} + \kappa\bar{\lambda}^2\bar{u}^2 = 0, \tag{3.65}$$

$$(\bar{\mathbf{v}}.\bar{\nabla})\bar{\mu} + \kappa\bar{\lambda}\bar{\mu}\bar{u}^2 = 0, \tag{3.66}$$

$$(\bar{\mathbf{v}}.\bar{\nabla})\bar{\nu} + \kappa\bar{u}^2\left(\bar{\mu}^2 - a^2\right) = 0, \tag{3.67}$$

$$\text{as } \bar{Y}\to\infty \qquad \bar{\lambda} \sim \frac{C_1}{\kappa^2C_0^2}(-\bar{X})^{-\frac{7}{16}}(2\bar{Y})^{-\frac{7}{8}}, \quad \bar{\mu} \sim C_2, \quad \bar{\nu} \sim \kappa^2C_0^2C_3(-\bar{X})^{\frac{7}{16}}(2\bar{Y})^{\frac{7}{8}}. \tag{3.68}$$

The equations (3.65)–(3.67) follow immediately from using (3.53) in (2.14)–(2.16) and keeping leading order terms. Here, at leading order, $\bar{u} = 2\kappa C_0(-\bar{X})^{\frac{1}{2}}, \bar{v} = \kappa C_0(-\bar{X})^{-\frac{1}{2}}\bar{Y}$. These equations have the explicit solution

$$\bar{\lambda} = \frac{(-\bar{X})^{-\frac{3}{2}}}{(-C_0)\kappa^2}\tilde{\lambda}(\xi), \qquad \bar{\mu} = \tilde{\mu}(\xi), \qquad \bar{\nu} = C_0\kappa^2(-\bar{X})^{\frac{3}{2}}\tilde{\nu}(\xi), \tag{3.69}$$

where

$$\bar{\lambda} = \frac{3}{4\left(1+3K_1\xi^{\frac{7}{8}}\right)}, \qquad \bar{\mu} = \frac{3K_1C_2\xi^{\frac{7}{8}}}{\left(1+3K_1\xi^{\frac{7}{8}}\right)}, \qquad \bar{\nu} = C_0C_3\xi^{\frac{7}{8}} + \frac{4K_1C_2^2\xi^{\frac{7}{8}}}{\left(1+3K_1\xi^{\frac{7}{8}}\right)} - \frac{4a^2}{3}, \tag{3.70}$$

with ξ as given in (3.62). The expressions (2.17) give

$$\bar{T}^p_{11} + \frac{\epsilon^{\frac{1}{2}}}{\mathrm{Wi}} = \bar{\lambda}\bar{u}^2 + O(\epsilon^{\frac{5}{7}}), \qquad \bar{T}^p_{12} = \bar{\lambda}\bar{u}\bar{v} + \epsilon^{\frac{3}{7}}\bar{\mu}, \qquad \bar{T}^p_{22} + \frac{\epsilon^{\frac{1}{14}}}{\mathrm{Wi}} = \bar{\lambda}\bar{v}^2 + \epsilon^{\frac{2}{7}}2\bar{\mu}\frac{\bar{v}}{\bar{u}} + \epsilon^{\frac{4}{7}}\frac{\bar{\nu}}{\bar{u}^2}. \tag{3.71}$$

At leading order we thus have

$$\bar{T}^p_{11} = \bar{\lambda}\bar{u}^2, \qquad \bar{T}^p_{12} = \bar{\lambda}\bar{u}\bar{v}, \qquad \bar{T}^p_{22} = \bar{\lambda}\bar{v}^2, \tag{3.72}$$

which gives (3.64) and justifies the choice of values $K_2 = K_3 = 0$ in (3.62). The expressions (3.71) show how further expansion terms are needed in the Cartesian formulation to capture the information carried by the μ and ν natural stress variables.

4 Discussion

The behaviour of the dimensional flow and stress variables may be summarised as follows. The velocity and pressure on the stick and slip interfaces $y = 0$ for $|x| \ll H$, may be summarised as follows

$$u = \frac{\partial\psi}{\partial y} = \begin{cases} 0, & x > 0, \\ 2\kappa C_0 V(-\frac{x}{H})^{\frac{1}{2}}, & x < 0, \end{cases} \qquad v = 0, \qquad p = \begin{cases} p_0\frac{(\eta_s+\eta_p)V}{H}\left(\frac{x}{H}\right)^{-\frac{1}{4}}, & x > 0, \\ 2\kappa C_0\frac{\eta_s V}{H}\left(-\frac{x}{H}\right)^{-\frac{1}{2}}, & x < 0, \end{cases} \tag{4.73}$$

whilst the polymer and solvent stresses are

$$\tau^p_{11} = \begin{cases} 2\frac{\eta_p V^{\frac{1}{2}}}{\lambda^{\frac{1}{2}}H^{\frac{1}{2}}}\left(\frac{1-\kappa}{\kappa}\right)^{\frac{1}{4}}|C_0|^{\frac{1}{2}}\left(\frac{x}{H}\right)^{-\frac{1}{4}}, & x > 0, \\ -3\frac{\eta_p V}{H}C_0\left(-\frac{x}{H}\right)^{-\frac{1}{2}}, & x < 0, \end{cases} \qquad \tau^p_{12} = \begin{cases} -\frac{\eta_p}{\lambda}\left(\frac{1-\kappa}{\kappa}\right)^{\frac{1}{2}}\frac{C_0}{|C_0|}, & x > 0, \\ 0, & x < 0, \end{cases}$$

$$\tau^p_{22} + \frac{\eta_p}{\lambda} = \begin{cases} \frac{\eta_p H^{\frac{1}{2}}}{\lambda^{\frac{3}{2}}V^{\frac{1}{2}}}\left(\frac{1-\kappa}{\kappa}\right)^{\frac{3}{4}}|C_0|^{-\frac{1}{2}}\left(\frac{x}{H}\right)^{\frac{1}{4}}, & x > 0, \\ 0, & x < 0, \end{cases} \tag{4.74}$$

$$\tau^s_{11} = -\tau^s_{22} = \begin{cases} 0, & x > 0, \\ -2\kappa\eta_s\frac{V}{H}C_0\left(-\frac{x}{H}\right)^{-\frac{1}{2}}, & x < 0, \end{cases} \qquad \tau^s_{12} = \begin{cases} 2\kappa\eta_s\frac{V}{H}C_0\left(\frac{x}{H}\right)^{-\frac{1}{2}}, & x > 0, \\ 0, & x < 0. \end{cases} \tag{4.75}$$

The first normal stress difference on the stick and slip surfaces near the singularity may be deduced as

$$N_1 = \begin{cases} 2\frac{\eta_p V^{\frac{1}{2}}}{\lambda^{\frac{1}{2}}H^{\frac{1}{2}}}\left(\frac{1-\kappa}{\kappa}\right)^{\frac{1}{4}}|C_0|^{\frac{1}{2}}\left(\frac{x}{H}\right)^{-\frac{1}{4}}, & x > 0, \\ (4\eta_s\kappa + 3\eta_p)\frac{V}{H}(-C_0)\left(-\frac{x}{H}\right)^{-\frac{1}{2}}, & x < 0. \end{cases}$$

Away from these surfaces we have in polar coordinates the velocity components

$$v_r = \kappa V C_0\left(\frac{r}{H}\right)^{\frac{1}{2}}f'(\theta), \qquad v_\theta = -\frac{3}{2}\kappa V C_0\left(\frac{r}{H}\right)^{\frac{1}{2}}f(\theta), \tag{4.76}$$

where $f(\theta) = 2\sin\left(\frac{\theta}{2}\right)\sin\theta$, with solvent and polymer stresses

$$\tau^s_{rr} = \kappa\frac{\eta_s V}{H}C_0\left(\frac{r}{H}\right)^{-\frac{1}{2}} f'(\theta), \quad \tau^s_{\theta\theta} = -\kappa\frac{\eta_s V}{H}C_0\left(\frac{r}{H}\right)^{-\frac{1}{2}} f'(\theta), \quad \tau^s_{r\theta} = \kappa\frac{\eta_s V}{H}C_0\left(\frac{r}{H}\right)^{-\frac{1}{2}}\left(f''(\theta)+\frac{3}{4}f(\theta)\right), \tag{4.77}$$

$$\tau^p_{rr} = \frac{\eta_p V}{H}C_1\left(\frac{r}{H}\right)^{-\frac{5}{16}}(f)^{-\frac{7}{8}} f'^2, \quad \tau^p_{\theta\theta} = -\frac{3}{2}\frac{\eta_p V}{H}C_1\left(\frac{r}{H}\right)^{-\frac{5}{16}}(f)^{-\frac{7}{8}} ff',$$

$$\tau^p_{r\theta} = \frac{9}{4}\frac{\eta_p V}{H}C_1\left(\frac{r}{H}\right)^{-\frac{5}{16}}(f)^{-\frac{7}{8}} f^2. \tag{4.78}$$

These give the local asymptotic behaviour of the Giesekus model at the stick-slip singularity. The velocity field is Newtonian, with solvent stresses dominating the polymer stresses apart from narrow regions at the stick and slip surfaces. This asymptotic structure holds for the parameter range $0 < \kappa < 1$ and $0 < \beta \leq 1$. It necessarily breaks down in the Oldroyd-B limit $\kappa \to 0^+$ as well as vanishing solvent viscosity $\beta \to 0^+$. The Newtonian limit $\beta \to 1^-$ poses no difficulty, with the influence of the polymer stresses clearly vanishing and the recovery of full Stokes flow.

A critical question that arises is the length scale on which this singular behaviour is expected to be obtained. The analysis uses a non-dimensional artificial parameter ϵ for representing the radial distances on which the asymptotic analysis holds. It's only analytical restriction being that it is small. Practically, numerical solution of the full equations is needed to determine how small ϵ needs to be, before this structure is obtained. However, for any given small distance from the singularity, the asymptotic structure indicated in Figure 2 may be used as a guide to the regions, their sizes and equation balances that have to be resolved by any given numerical scheme.

References

[1] P. Andre and J.-R Clermont, Numerical simulation of the die swell problem of a Newtonian fluid by using the conceptof stream function and a local analysis of the singularity at the corner, *J. Non-Newtonian Fluid Mech.* **23** (1987), 335–357.

[2] M.R. Apelian, R.C. Armstrong and R.A. Brown, Impact of the constitutive equation and singularity on the calculation of stick-slip flow: The Modified Upper-Convected Maxwell Model (MUCM), *J. Non-Newtonian Fluid Mech.* **27** (1988), 299–321.

[3] R.B. Bird, C.F. Curtiss, R.C. Armstrong and O. Hassager, *Dynamics of Polymeric Liquids*, vol. 2, 2nd edition. *Wiley-Intersciences, New York* 1987.

[4] A.N. Bris, R.C. Armstrong and R.A. Brown, Finite element calculation of viscoelastic flow in a journal bearing. II. Moderate eccentricity, *J. Non-Newtonian Fluid Mech.* **19** (1988), 323–347.

[5] M.M. Denn, Extrusion instabilities and wall slip, *Annu. Rev. Fluid Mech.* **33** (2001), 265–287.

[6] J.D. Evans, Re-entrant corner flow of PTT fluids with a solvent viscosity, *J. Non-Newtonian Fluid Mech.* **165** (2010), 527–537.

[7] J.D. Evans, Re-entrant corner behaviour of the Gieskus fluid with a solvent viscosity, *J. Non-Newtonian Fluid Mech.* **165** (2010), 538–543.

[8] J.D. Evans, Stick-slip and slip-stick singularities of the Phan-Thien–Tanner fluid, *J. Non-Newtonian Fluid Mech.* **199** (2013), 12–19.

[9] M.A. Fontelos and A. Friedman, Analysis of the stick-slip problem for non-Newtonian flows. *Comm. Partial Differential Equations.* **26** (2001), 461–536.

[10] A. Fortin, A. Zine and J-F. Agassant, Computing viscoelastic fluid flow problems at low cost, *J. Non-Newtonian Fluid Mech.* **45** (1992), 209–229.

[11] G.C. Georgiou, L.G. Olson, W.W. Schultz and S. Sagan, A singular finite element for Stokes flow: The stick-slip problem. *Int. J. Num. Methods Fluids.* **9** (1989), 1353–1367.

[12] H. Giesekus, A simple constitutive equation for polymer fluids based on the concept of deformation-dependent tensorial mobility. *J. Non-Newtonian Fluid Mech.* **11** (1982), 69–109.

[13] H. Giesekus, A unified approach to a variety of constitutive models for polymer fluids based on the concept of configuration dependent molecular mobility. *Rheol. Acta.* **21** (1982), 366–375.

[14] H. Giesekus, Stressing behaviour in simple shear flow as predicted by a new constitutive model for polymer fluids. *J. Non-Newtonian Fluid Mech.* **12** (1983), 367–374.

[15] T. Hagen and M. Renardy, *Boundary layer analysis of the Phan-Thien-Tanner and Giesekus model in high Weissenberg number flow*, *J. Non-Newtonian Fluid Mech.* **73** (1997), 181–189.

[16] G. Karapetsas and J. Tsamopoulos, On the stick-slip flow from slit and cylindrical dies of a Phan-Thien and Tanner fluid model. I. Steady state, *Phys. Fluids* **21** (2009), 123101.

[17] G. Karapetsas and J. Tsamopoulos, On the stick-slip flow from slit and cylindrical dies of a Phan-Thien and Tanner fluid model. II. Linear stability analysis, *Phys. Fluids* **25** (2013), 093105.

[18] R.C. King, M.R. Apelian, R.C. Armstrong and A.B. Brown, *Numerically stable finite element techniques for viscoelastic calculations in smooth and singular geometries*, *J. Non-Newtonian Fluid Mech.* **29** (1988), 147–216.

[19] R.G. Larson, *Constitutive Equations for Polymer Melts and Solutions*, *Butterworths* 1988.

[20] G.G. Lipscomb, R. Keunnings and M.M. Denn, *Implications of boundary singularities in complex geometries*, *J. Non-Newtonian Fluid Mech.* **24** (1987), 85–96.

[21] MATLAB version 7.11.0. (R2010b) Natick, Massachusetts, *The MathWorks Inc.* (2010).

[22] D.H. Michael, The separation of a viscous liquid at a straight edge, *Mathematika* **5** (1958), 82–84.

[23] H.K. Moffatt, Viscous and resistive eddies near a sharp corner, *J. Fluid Mech.* **18** (1964), 1–18.

[24] V. Ngamaramvaranggul and M.F. Webster, Viscoelastic simulations of stick-slip and die-swell flows, *Int. J. Numer. Methods Fluids.* **36** (2001), 539–595.

[25] M. Renardy, How to integrate the upper convected Maxwell (UCM) stresses near a singularity (and maybe elsewhere, too), *J.Non-Newtonian Fluid Mech.* **52** (1994), 91–95.

[26] M. Renardy, The high Weissenberg number limit of the UCM model and the Euler equations, *J. Non-Newtonian Fluid Mech.* **69** (1997), 293–301.

[27] S. Richardson, *A stickslip problem related to the motion of a free jet at low Reynolds numbers*, *Proc. Camb. Phil. Soc.* **67** (1970), 477–489.

[28] T.R. Salamon, D.E. Bornside, R.C. Armstrong and R.A. Brown, Local similarity solutions for the stress field of an Oldroyd-B fluid in the partial-slip/slip flow, *Phys. Fluids.* **9** (1997), 2191.

[29] G. Schleiniger and R.J. Weinacht, *A remark on the Giesekus viscoelastic fluid*, *J. Rheol.* **35** (1991), 1157–1170.

[30] W.J. Silliman and L.E. Scriven, *Separating flow near a static contact line. Slip at a wall and shape of a free surface*, *J. Comput. Phys.* **34** (1980), 287–313.

[31] V.A. Solonnikov, *Problèm de frontiére libre dans l'ecoulement d'un fluide á la sortie d'un tube cylindrique*, *Asymptotic Analysis.* **17** (1998), 135–163.

[32] R. I. Tanner, A theory of die-swell, *J. Polym. Sci. A-2* **8** (1970), 2067–2078.

[33] R. I. Tanner, *Engineering Rheology*, *OUP* 1985.

[34] R. I. Tanner, A theory of die-swell revisted, *J. Non-Newtonian Fluid Mech.* **129** (2005), 85–87.

[35] R. I. Tanner and X. Huang, Stress singularities in non-Newtonian stickslip and edge flows, *J. Non-Newtonian Fluid Mech.* **50** (1993), 135–160.

[36] S.A. Trogdon and D.D. Joseph, The stick-slip problem for a round jet. 1. Large surface tension, *Rheol. Acta.* **19** (1980), 404–420.